

UGC8802: A MASSIVE DISK GALAXY IN FORMATION

SEAN M. MORAN¹, GUINEVERE KAUFFMANN², TIMOTHY M. HECKMAN¹, JAVIER GRACIA-CARPIO³, AMELIE SAINTONGE³,
BARBARA CATINELLA¹, JING WANG¹, YAN-MEI CHEN¹, LINDA TACCONI³, DAVID SCHIMINOVICH⁴, PIERRE COX⁵, RICCARDO
GIOVANELLI⁶, MARTHA HAYNES⁶, AND CARSTEN KRAMER⁷

(Accepted July 19, 2010)
Draft version June 18, 2018

ABSTRACT

We report new observations of the galaxy UGC8802 obtained through GASS, the GALEX Arecibo SDSS Survey, which show this galaxy to be in a remarkable evolutionary state. UGC8802 (GASS35981) is a disk galaxy with stellar mass $M_* = 2 \times 10^{10} M_\odot$ which appears to contain an additional $2.1 \times 10^{10} M_\odot$ of HI gas. New millimeter observations with the IRAM 30m telescope indicate a molecular gas mass only a tenth this large. Using deep long-slit spectroscopy, we examine the spatially resolved star formation rate and metallicity profiles of GASS35981 for clues to its history. We find that the star formation surface density in this galaxy is low ($\Sigma_{\text{SFR}} = 0.003 M_\odot \text{ yr}^{-1} \text{ kpc}^{-2}$) and that the star formation is spread remarkably evenly across the galaxy. The low molecular gas masses measured in our three IRAM pointings are largely consistent with the total star formation measured within the same apertures. Our MMT long-slit spectrum reveals a sharp drop in metallicity in the outer disk of GASS35981. The ratio of current star formation rate to existing stellar mass surface density in the outer disk is extremely high, implying that all the stars must have formed within the past ~ 1 Gyr. At current star formation rates, however, GASS35981 will not consume its HI reservoir for another 5-7 Gyr. Despite its exceptionally large gas fraction for a galaxy this massive, GASS35981 has a regular rotation curve and exhibits no sign of a recent interaction or merger. We speculate that GASS35981 may have acquired its gas directly from the inter-galactic medium, and that it and other similar galaxies identified in the GASS survey may provide rare local glimpses of gas accretion processes that were more common during the prime epoch of disk galaxy formation at $z \sim 1$.

Subject headings: galaxies: individual (UGC8802) – galaxies: star formation – galaxies: evolution – galaxies: ISM – galaxies: stellar content – galaxies: kinematics and dynamics

1. INTRODUCTION

One of the largest gaps in our understanding of how galaxies form and evolve is the question of how gas—the raw material for star formation—flows into and out of galaxies, and how these flows regulate star formation in these systems. Although Λ CDM simulations make specific predictions for how structure in the dark matter assembles through hierarchical clustering, the assembly of the visible, baryonic components of galaxies is still a subject of considerable controversy.

The currently favored theoretical picture is that cold gas flows along filaments into the centers of assembling dark matter halos at high redshifts ($z > 2$), and this process can build massive galaxies rapidly at early times (e.g., Genel et al 2008; Dekel et al 2009). At lower redshift, massive spiral galaxies are thought to accrete gas much more slowly, at a rate of less than a few solar

masses per year, from a surrounding hot corona (Maller & Bullock 2004; Kauffmann et al 2006; Peek, Putman & Sommer-Larsen 2008; Binney, Nipoti & Fraternali 2009). Gas may also continue to accrete through major or minor mergers with other galaxies, although this is not believed to be the primary way in which ongoing star formation in local spiral galaxies is fuelled at present (Sancisi et al. 2008). Outflows, whether from star-formation or AGN-related feedback mechanisms, are another piece of the puzzle, and their role in shutting down star formation, limiting the efficiency with which stars are able to form, or even providing fuel for ongoing star formation in the form of recycled wind material (Oppenheimer et al. 2009), is similarly debated.

In order to learn more about cold gas in nearby galaxies, we are carrying out the GALEX Arecibo SDSS Survey (GASS)⁸ (Catinella et al. 2010). GASS is designed to measure the neutral hydrogen content of a representative sample of ~ 1000 galaxies uniformly selected from the SDSS spectroscopic and GALEX imaging surveys, with stellar masses in the range $10^{10} - 10^{11.5} M_\odot$ and redshifts in the range $0.025 < z < 0.05$. As GASS observations are designed to detect HI down to a gas-fraction limit of 1.5%, the full GASS sample will be the first HI survey able to place meaningful, unbiased constraints on the atomic gas reservoirs that may contribute to future growth in massive galaxies.

We are also pursuing a companion project on the

moran@pha.jhu.edu

¹ Department of Physics and Astronomy, The Johns Hopkins University, 3400 N. Charles Street, Baltimore, MD 21218, USA

² Max Planck Institut für Astrophysik, Karl-Schwarzschild-Str. 1, D-85741 Garching, Germany

³ Max Planck Institut für Extraterrestrische Physik, Giessenbach-Str., 85748 Garching, Germany

⁴ Department of Astronomy, Columbia University, 550 West 120th Street, New York, New York 10027, USA

⁵ Institut de RadioAstronomie Millimétrique, 300 rue de la Piscine, 38406 Saint Martin d'Hères, France

⁶ Department of Astronomy, 610 Space Sciences Building, Cornell University, Ithaca, NY 14853, USA

⁷ Instituto de RadioAstronomía Milimétrica, Avenida Divina Pastora, 7, E 18012 Granada, Spain

⁸ <http://www.mpa-garching.mpg.de/GASS>

IRAM 30m telescope, COLD GASS⁹, which will obtain accurate and homogeneous molecular gas masses for a subset of ~ 300 galaxies from the GASS sample. These data will allow us to characterize the balance between atomic and molecular gas in the galaxies in our sample, and understand the physical processes that determine how the condensed baryons are partitioned into stars, HI and H₂ in the local Universe.

In this paper, we report on UGC8802, an extraordinary galaxy blindly selected for inclusion in the GASS sample (under the catalog name GASS35981, used hereafter), which contains a reservoir of HI $> 10^{10} M_{\odot}$, at least equal in mass to the galaxy’s entire stellar content. This galaxy contains less than one tenth this mass in H₂ and also has a rather modest star formation rate (SFR). We describe the spectroscopic follow-up that enables us to conclude that the outer disk of this galaxy is currently forming from gas that has likely accreted from the external environment. In the following, we adopt a standard Λ CDM cosmology with $H_0 = 70 \text{ km s}^{-1} \text{ Mpc}^{-1}$, $\Omega_m = 0.3$ and $\Omega_{\Lambda} = 0.7$.

2. OBSERVATIONS

GASS35981 (also SDSS J135308.36+354250.5, in addition to UGC8802), was selected for inclusion in the GASS parent sample because it has photometry from both SDSS and GALEX, is located in a region of sky accessible to Arecibo, and has stellar mass of $M_{*} = 2 \times 10^{10} M_{\odot}$ and redshift of $z = 0.0411$ that fit into our targeted range. GASS35981 has pre-existing HI observations available from the Cornell HI Digital Archive (Springob et al. 2005). The mass of HI in GASS35981 is estimated from the line flux to be $2.1 \times 10^{10} M_{\odot}$, and the rest-frame velocity width of the HI line is $W_{50} = 360 \pm 25 \text{ km s}^{-1}$ (Figure 1). We display the HI archive spectrum in Figure 1. We note that there is no evidence for contamination from possible companion galaxies within the $3.5'$ Arecibo beam: one nearby galaxy has a spectroscopic redshift of 0.14, and two additional faint companions have SDSS photometric redshifts consistent with $z = 0.14$.

The lower panel of Figure 1 shows that GASS35981 (blue star) lies near the extreme end of HI fractions observed by GASS. Indeed, its gas fraction is comparable to the highest values measured for all galaxies in this stellar mass range (e.g., Giovanelli et al. 2007). Indeed, even in HI-selected samples, which are biased towards objects like GASS35981, galaxies in this stellar mass range ($M_{*} > 10^{10} M_{\odot}$) with such high gas fractions are quite uncommon (e.g., the ‘‘HI Giants’’ described by Garcia-Appadoo et al. 2009).

It is also clear that GASS35981 lies significantly above the best-fit ‘gas fundamental plane’ (dotted line) relating stellar mass surface density, NUV- r color, and gas fraction, as described in Catinella et al. (2010). Because this galaxy was an interesting outlier and a presumed easy target, GASS35981 was selected for inclusion in our initial COLD GASS pilot program to obtain molecular gas measurements with the IRAM 30m telescope.

Observations of GASS35981 in the J=1-0 rotational transition of CO were made at 3mm with the IRAM 30m telescope, in three different pointings: one at the galaxy center, and one each to the north and south, one beam-

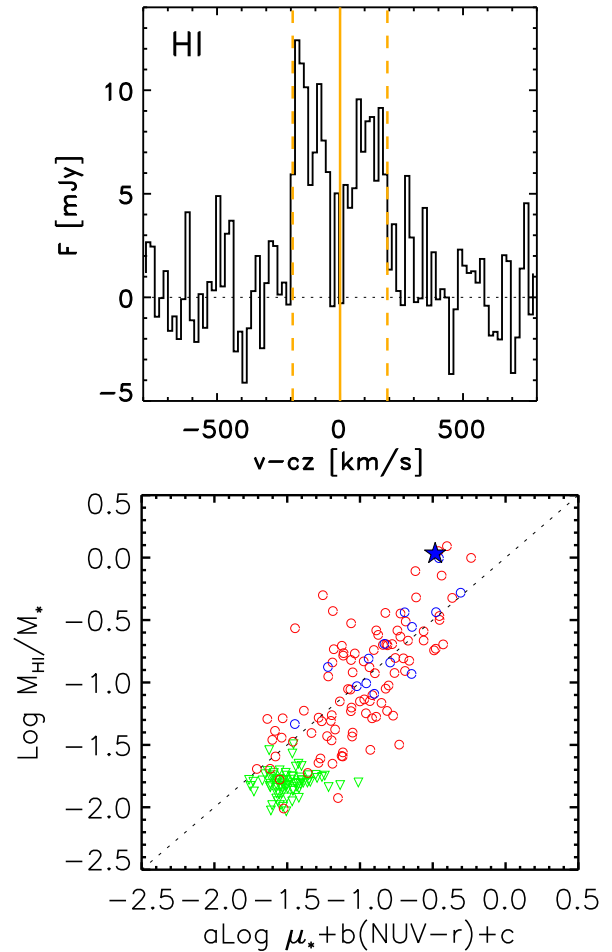


Figure 1. Top: HI spectrum of GASS35981 from the Cornell HI Digital Archive (Springob et al. 2005). The solid orange line indicates the measured HI line center, and the dashed lines mark the velocity width of the spectrum. Bottom: GASS35981 on the ‘gas fundamental plane’ presented in Catinella et al. (2010), relating HI mass fractions to stellar mass surface density (μ_{*}) and NUV- r color. The best-fit values of the coefficients a , b , and c used in constructing the plane are: $a = -0.332$, $b = -0.240$, and $c = 2.856$. GASS35981 is marked with a blue star. Red circles indicate HI-detected galaxies from GASS, and green triangles mark upper limits on gas fraction. Blue circles denote a set of galaxies randomly drawn from previous HI surveys, and added to the GASS galaxies in the proper proportion to generate a statistically unbiased sample (see Catinella et al. (2010)).

width ($22''$) away along the galaxy major axis. Data were taken in June and August 2009, using the WILMA and 4MHz backends simultaneously to record the data, and the CLASS¹⁰ software to process them. Individual scans were examined, and a linear baseline subtracted from each of them. After rejection of scans with unstable baselines due to, e.g., poor atmospheric conditions, the data were combined and binned to a spectral resolution of 21 km s^{-1} .

The CO line is detected in the central pointing with $S/N = 5.8$, for an integrated line flux of $T_a^{*} = 0.43 \pm 0.07 \text{ K km s}^{-1}$ within a 400 km s^{-1} -wide window. We set upper limits at 0.29 and 0.43 K km s^{-1} for the North and South offset pointing, respectively. Adopting a conversion factor of $X_{CO} = 4.4 M_{\odot}/L'$ (where L' has units of

⁹ http://www.mpa-garching.mpg.de/COLD_GASS

¹⁰ <http://www.iram.fr/IRAMFR/GILDAS>

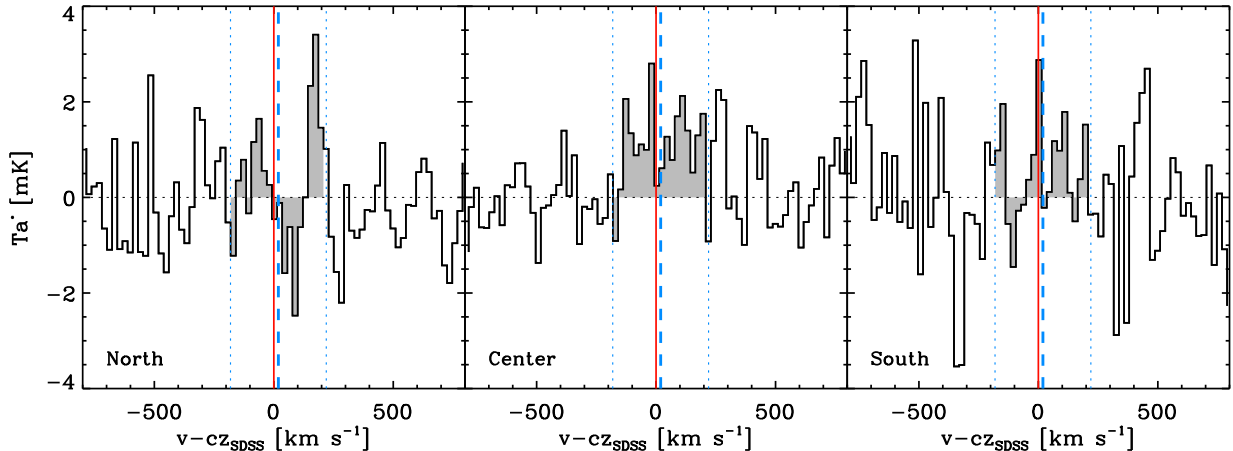


Figure 2. CO spectra for all three IRAM pointings, as labeled on the figure. The red lines mark the optical redshift of GASS35981, the blue dashed lines show the velocity centroid of the central CO emission, and the dotted lines represent the width of the window function that was used to measure the flux in the CO lines, covering an area marked by grey shading under the spectrum. In the central pointing, the peak at ~ 300 km s $^{-1}$ is believed to be noise, as it does not appear in both polarizations; it therefore is excluded from our measurement.

K km s $^{-1}$ pc $^{-2}$), these fluxes correspond to an H $_2$ mass of $8.8 \times 10^8 M_\odot$ in the central 22'' pointing, and upper limits of 5.9 and $8.8 \times 10^8 M_\odot$ in the offset pointings. Using an aperture correction for the 22'' beam of the IRAM telescope based on resolved CO maps of nearby galaxies, we estimate a total H $_2$ mass of $1.45 \times 10^9 M_\odot$ for the galaxy, based on the detection in the central pointing. Following the prescription of Springob et al. (2005), we measure a line width of $W_{50} = 335 \pm 20$ km s $^{-1}$. This corresponds to a rest-frame width of 321 km s $^{-1}$. The spectra of all three pointings are shown in Figure 2.

Follow-up long-slit spectroscopy of GASS35981 was obtained on 20 November, 2009, using the Blue Channel Spectrograph on the 6.5m MMT telescope on Mt. Hopkins, AZ. The spectrum was obtained with a slit of width 1.25'' oriented to PA = 13.4° on the sky, such that the slit runs along the major axis of the galaxy, as indicated in the second panel of Figure 3. GASS35981 was observed in 2x600s exposures with the 500 line grating. The spectrum covers a wavelength range of $\sim 3900 - 7000 \text{ \AA}$ at a spectral resolution of $\sim 4 \text{ \AA}$ FWHM, equivalent to $\sigma \sim 75$ km s $^{-1}$ in the rest frame of the galaxy. The slit samples the galaxy spatially with 0.3 pixels (equivalent to 0.25 kpc in physical units), over a total slit length of 150'', which is much larger than the galaxy itself.

Data were reduced in IDL with routines from the publicly available Low-Redux package¹¹ maintained by X. Prochaska, which itself is an adaptation of the Princeton SDSS reduction code¹² to more general long-slit reductions. The code performs standard biasing, flat-fielding, cosmic-ray rejection, and sky estimation on each exposure. We then co-add the sky-subtracted exposures through a custom-written routine that verifies and adjusts the alignment of exposures before co-addition. Flux calibration was achieved via observation of the spectrophotometric standard BD+17 4708. We note that we have not attempted to apply any correction for atmospheric dispersion, even though GASS35981 was observed at an airmass of 1.8. The expected atmospheric dispersion from blue to red end for our configuration, as

estimated from Filippenko & Greenstein (1984), is comparable to the size of our slit. More importantly, it is much smaller than the typical spatial regions we average over in the analysis presented below. A cut-out of the fully-reduced spatially-resolved spectrum centered on the H α emission line, including only that portion of the slit where significant flux from the galaxy is detected, is displayed in Figure 3.

3. ANALYSIS

To understand why GASS35981 contains such a high abundance of HI, but little molecular gas, we analyze our long-slit spectrum with an eye toward extracting information on the dynamics of the galaxy and the properties of its stellar population—including current star formation rate, stellar population age and metallicity, and dust properties—as a function of radius across the galaxy. We likewise re-analyze the SDSS *ugriz* and GALEX FUV and NUV images of GASS35981 to obtain independent estimates of the radial gradients in colors and star formation histories, as described below.

3.1. Rotation Curve

To measure the rotation curve of GASS35981, we first bin our spectrum spatially to achieve a signal to noise of at least 6.0 (\AA^{-1}) in each bin, the minimum needed for a reliable velocity estimate. We define spatial bins by working outward from the galaxy center (where S/N is high even without binning), co-adding rows one at a time until the minimum S/N is reached, or until adding rows fails to increase the S/N. Since strong H α emission is detected in GASS35981 out to much larger radius than the continuum flux (see Figure 3), we also include several additional bins that correspond to knots of bright H α emission in the spectrum. For each binned spectrum, we determine the effective spatial position by calculating the luminosity-weighted average radius of all spatial positions that entered the co-add.

We then measure the radial velocity as a function of radius in two ways: 1) by cross-correlating each spectrum against galaxy templates to determine the velocity, 2) by fitting directly for the centroids of the H α emission line. The method utilizing H α allows us to extend our

¹¹ <http://www.ucolick.org/~xavier/LowRedux/>

¹² <http://spectro.princeton.edu>

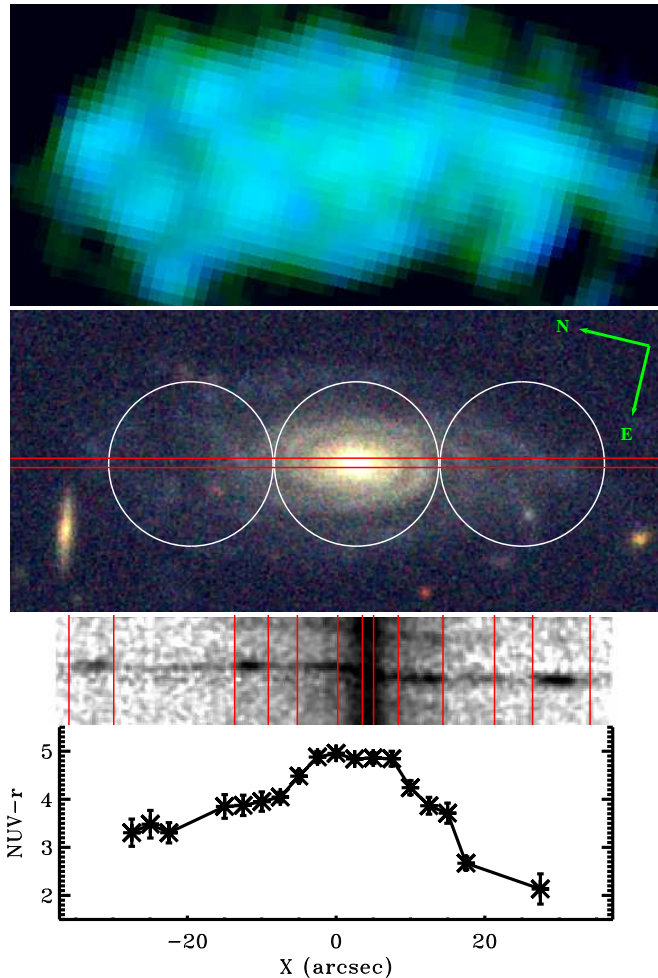


Figure 3. **Top:** GALEX UV image of GASS35981 with FUV in blue and NUV in green, smoothed by a Gaussian with FWHM $3.5''$, slightly smaller than the GALEX psf of $4.5''$. The dimensions of the image are $87''$ wide by $42''$ tall. **Upper Middle:** Color SDSS image of GASS35981 constructed from *gri* images, and displayed at the same scale and size as the GALEX image above. Orientation and width of the spectroscopic slit are overlaid in red, with north indicated by the compass rose. White circles overlaid indicate the three IRAM CO pointings, with circle diameter equal to the $22''$ FWHM IRAM beam size. **Lower Middle:** A cutout of the spectrum around the region of the $H\alpha$ emission line is shown at the same spatial scale along the x-axis. Bright $H\alpha$ knots can be clearly associated with faint blue regions of the outer galaxy that intersect the slit. Vertical red lines mark out the twelve spatial regions over which we have co-added our spectrum. All spectroscopic measurements in this paper are measured on these twelve spectra. **Bottom:** $NUV-r$ color profile of GASS35981 extracted from a region overlapping our slit. Note that the X-axis arcsecond scale applies to all four panels of this figure.

rotation curves to larger radii. The two methods yield consistent curves at radii where we can fit templates and measure emission line centroids. The resulting rotation curve is plotted in Figure 4, not corrected in any way for the inclination of the galaxy. The solid line plotted over the measured curve is the best-fitting rotation curve of the form $V(R) = V_{\text{MAX}}R/(R^a + R_s^a)^{1/a} + \Delta V$ (Bøhm et al. 2004; Moran et al. 2007), where R is the radius, a and R_s are free parameters that govern the shape of the rotation curve and its turn-over, and ΔV is the offset of the galaxy’s central velocity from the redshift obtained from the SDSS spectrum (also left as a free parameter). We measure a circular velocity for

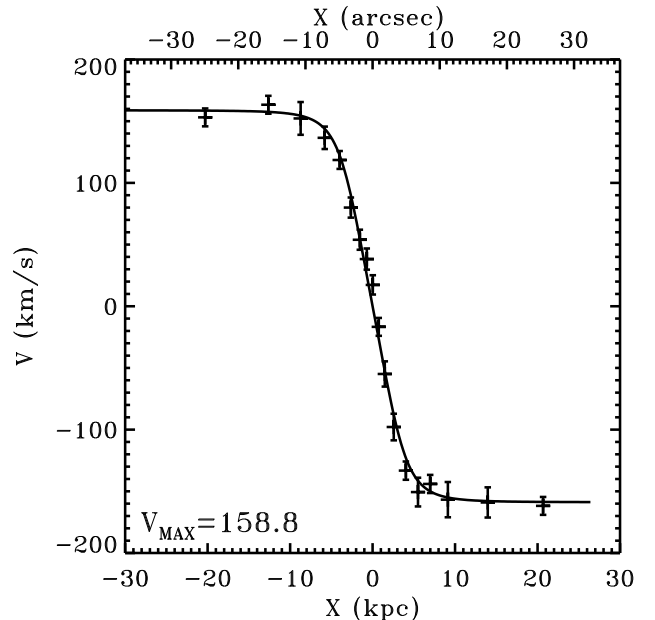


Figure 4. Rotation curve of GASS35981 measured primarily from cross-correlation of the spectrum to templates, supplemented by measurements of the $H\alpha$ centroid for the two outermost bins to each side. Solid line indicates the best-fitting model of the form described in the text, which is symmetric to positive and negative positions.

GASS35981 of $2V_{\text{MAX}} = 318 \pm 10 \text{ km s}^{-1}$. This is consistent with the value obtained from the CO spectrum ($W = 321 \pm 10 \text{ km s}^{-1}$).

Table 1 summarizes some of the basic properties of GASS35981, including the masses and line widths of the various components. The agreement between CO and $H\alpha$ widths is not surprising because at the radius of the IRAM beam (11 arcsec), the optical velocity has already reached its maximum value. It is interesting, however, that the rest-frame HI velocity width, $W = 360 \pm 25 \text{ km s}^{-1}$, appears to be somewhat larger than the estimates from both CO and $H\alpha$.¹³ Since the optical rotation curve of GASS35981 is flat, one might have expected a better agreement between the HI and $H\alpha$ widths.

Even though the significance of the difference is marginal (smaller than 2σ), it is interesting to comment on possible causes of the effect. Based on a statistical analysis of a large data set with both $H\alpha$ and HI spectroscopy, Catinella et al. (2007) find a systematic difference between optical and HI velocities of normal spiral galaxies with flat rotation curves of a factor 1.06 (see their figure 6). After applying a 6.5 km s^{-1} turbulent motion correction (as in Catinella et al. 2007), and accounting for such a scaling factor, the HI width of GASS35981 is 333 km s^{-1} , which is in slightly better agreement with the optical rotation curve and CO linewidth. The residual difference might be explained by uncertain statistical and turbulent motion corrections, or it might provide evidence for accretion of HI at large radii. It is interesting that the HI profile shown in Fig-

¹³ We note that the velocity widths are not deprojected to edge-on (the galaxy’s inclination is 63.25 degrees from face-on, estimated as $\cos(i) = b/a = 0.45$).

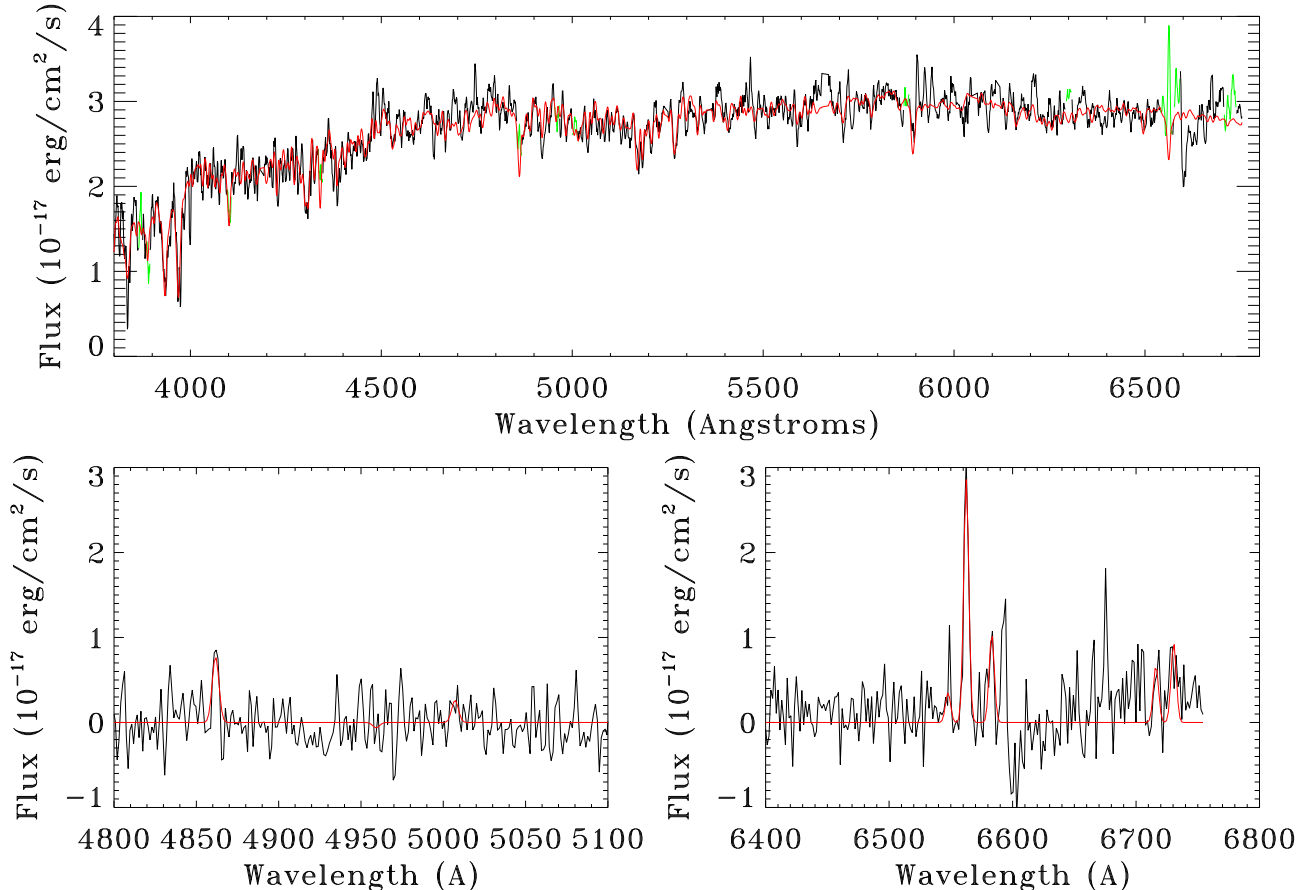


Figure 5. Example of absorption template (top) and emission line (bottom) fits to the observed spectrum of GASS35981, here shown for a spectrum extracted 2–3kpc from the center of the galaxy. In the top panel, the spectrum is plotted in black with regions that were masked for the fitting indicated in green. The best-fitting model spectrum is over-plotted in red. In the bottom two panels, two cutouts of the spectrum near the $H\beta$ and $H\alpha$ emission lines are replotted with the best-fit model subtracted off. Our Gaussian fits to key emission lines are then over-plotted in red.

ure 1 is noticeably asymmetric. We will come back to this point in the final discussion.

3.2. Spatial Binning of the Spectrum

We now correct each row in the unbinned 2D spectrum to a common rest-frame using the rotation curve in Figure 4. This procedure is necessary if we wish to obtain accurate measurements of spectral lines. We then re-bin the spectrum to a slightly higher targeted S/N of ~ 8 . To each side, the two bins at highest radii are chosen by hand, because there is no clear detection of the stellar continuum this far out. As can be seen in Figure 3, nebular emission is still clearly detected in these regions, so we choose the binning to correspond to clear transitions between the bright or faint knots of $H\alpha$. We end up with a total of 12 radial bins, and we mark the limits of each with red lines on the spectrum in Figure 3. We use this re-binned spectrum in our subsequent analysis.

3.3. Continuum & Emission Line Fitting

We employ a modified version of the technique of Brinchmann et al (2004) to measure the strengths of key emission and absorption lines as a function of radius across GASS35981. The spectrum from each of our 12 spatial positions is first fit to a linear combination of templates drawn from Bruzual & Charlot (2003) single stellar population models, masking regions of the

spectrum occupied by common emission lines. Best-fit model spectra are generated individually for both a low- and high-metallicity set of Bruzual & Charlot models ($0.02Z_{\odot}$ and Z_{\odot} , respectively), and we retain the one with lowest reduced χ^2 of the fit. Near the center of the galaxy, these fits unambiguously favor the solar-metallicity model. Low-metallicity templates provide a slightly better fit in each of the two outermost bins where we can measure the stellar continuum ($R \sim 15$ kpc on each side). However, we caution that the S/N in the continuum is < 5 here, and so the best-fitting metallicity is unlikely to be a reliable indicator. The results of an example fit are shown in Figure 5.

Next, we subtract the best-fitting stellar continuum model from the measured spectrum, creating an emission-line only spectrum where the Balmer emission lines can be measured free of contamination from the underlying stellar absorption. In the two outermost bins, only nebular emission is detected and no continuum fitting is possible. In these cases, we fit a low-order polynomial to the spectrum to correct for small imperfections in our sky subtraction, which arise when co-adding across a large portion of the slit. We then measure emission lines using the polynomial-subtracted spectrum.

We fit a Gaussian function to the emission lines, with the width of the Gaussian constrained to a single value

Table 1
GASS35981 Key Properties

M_*	$2.0 \pm 0.3 \times 10^{10} M_\odot$	$W_{H\alpha}^b$	$318 \pm 10 \text{ km s}^{-1}$
M_{HI}^a	$2.1 \pm 0.4 \times 10^{10} M_\odot$	$W_{HI}^{a,b}$	$360 \pm 25 \text{ km s}^{-1}$
M_{CO}	$1.4 \pm 0.2 \times 10^9 M_\odot$	W_{CO}^b	$321 \pm 19 \text{ km s}^{-1}$
M_r	-21.2	M_{NUV}	-18.7
R_{25}^c	24 kpc	R_e^d	9.8 kpc
z	0.0411	$SFR_{H\alpha}$	$3.7 \pm 0.3 M_\odot$

^a Springob et al. (2005)

^b Rest-frame line width

^c SDSS r -band isophotal major axis radius (25mag $''^2$)

^d SDSS r -band Petrosian half-light radius

for all lines in a given spectrum. The positions of the line centroids are constrained to their rest-wavelengths. The only free parameters in the fit are the amplitude of each line and an overall velocity offset term. For each line, we also recalculate the continuum level in a small region within 50Å of each fitted line, and subtract this small residual from the template fits to further refine the measured emission line flux. In addition to the Balmer lines H α , H β , and H γ , used to estimate dust extinction and star formation rate (see below), we also measure the forbidden lines [OIII] 5007, [NII] 6548 and 6584, and [SII] 6717 and 6731 to measure metallicity across the galaxy.

We limit our analysis of stellar absorption features to the $D4000_n$ index, which measures the strength of the 4000Å break. This index is an indicator of stellar population age (see, e.g., Kauffmann et al. 2003). We use $D4000_n$ values measured from the best-fitting absorption line templates, rather than from the spectrum itself. The two agree well for spectral bins with high S/N. We choose the model measurement as we expect it to yield a more reliable estimate in bins where S/N in the continuum is only $\sim 3 - 5$, because the model fit utilizes information from the entire spectrum.

We estimate the dust extinction within the nebular gas by calculating the Balmer decrement, which we define as the ratio of H α /H β to the case B recombination ratio of 2.87 (Osterbrock 1989). We adopt the formula $A_V = 1.9655 R_V \log(H\alpha/H\beta/2.87)$, where we assume $R_V = 3.1$ and adopt the Calzetti (2001) extinction curve. We further refine the estimates of A_V by comparing to the H γ line, which is only strong enough to be measured in emission in a few cases. However, even as an upper limit, H γ provides a useful constraint. If, after correcting all three lines for dust based on our original A_V estimate, the ratios H γ /H α and/or H γ /H β are *inconsistent* with the expected values of 0.474 and 0.166, respectively, we adjust A_V upward or downward—staying within the 1σ errors on the original measurement—to improve the agreement with these values as far as possible.

We note that all SFRs reported below have been calculated after correcting fluxes for extinction using the Balmer decrement. Likewise, our equivalent widths have been corrected for dust using our measured Balmer decrements and assuming E(B-V) of the stellar light is ~ 0.44 E(B-V) of the gas, as in Calzetti (2001).

3.4. Colors and Star Formation Rates from the Photometry

We measure the UV/optical color profiles of GASS35981 using SDSS and GALEX photometry in two ways. First, we measure fluxes in a 5'' wide strip running along the major axis of the galaxy. Our chosen aperture lies on top of, but is wider than the spectroscopic slit. To ensure that the fluxes measured using the SDSS images are well-matched to those measured from the GALEX images, we convolve the SDSS images with a Gaussian of FWHM 4.5'' (the size of the GALEX PSF). The resulting color profile is displayed in the bottom panel of Figure 3.

For more precise comparison to the spectroscopy (but at the expense of lower S/N in lower surface brightness regions), we also measured colors through apertures with widths identical to the slit segments containing each of our twelve spectral bins. These apertures are smaller than the GALEX PSF, so we scale the SDSS u -band flux measured in the smaller apertures by the ratio of FUV or NUV to u measured in the wider aperture at the same position along the slit. We use these measurements to estimate SFR and stellar mass surface densities by fitting the full UV through optical SEDs to population synthesis models as described in Wang et al. (2010, in preparation). Our method is very similar to that described in Salim et al. (2007).

To optimize the fits, we constrain the internal extinction of the galaxies in the library of models to be consistent with the measured Balmer-decrement values for this galaxy. Assuming that the attenuation of the starlight is 0.44 times the extinction measured in nebular gas (Calzetti 2001), we obtain $\tau_v = 0.5$ averaged over our 12 spectral bins, with a dispersion of ± 0.25 . We use this as a prior in our parameter estimation.

4. RESULTS

In this section, we analyse star formation rates, stellar population ages and metallicities of the nebular gas as a function of position in GASS35981. We show that star formation is spread fairly evenly across the disk of the galaxy, but the ratio of current star formation to stellar mass surface density in the outskirts of the galaxy is very high. This suggests the outer disk has been formed recently. We then show that the modest H $_2$ content implied by the CO observations matches expectations from the star formation rate profile of the galaxy. We also examine the metallicity profiles, finding a sharp drop in metallicity that corroborates our conclusion that stars in the outer disk were formed recently.

4.1. Star Formation in GASS35981

After correcting H α luminosities for dust, we measure star formation rates using the equation in Meurer et al. (2009): $SFR (M_\odot \text{ yr}^{-1}) = L_{H\alpha} / (6.93 \times 10^{33} \text{ W})$, corrected to a Kroupa (2001) IMF. Then, by dividing by the area of the galaxy covered by each portion of the slit ($1.25'' \times 0.3'' N$, where N is the number of individual rows that went into each co-added spectrum), we estimate the SFR surface density as a function of position across GASS35981. This is shown in Figure 6, left, from which it is clear that the SFR surface density is remarkably uniform across the galaxy. This result is confirmed by the SFR surface densities estimated from the photometry alone (§ 3.3), over-plotted as red circles on Figure 6, which match the values estimated using the spectroscopy

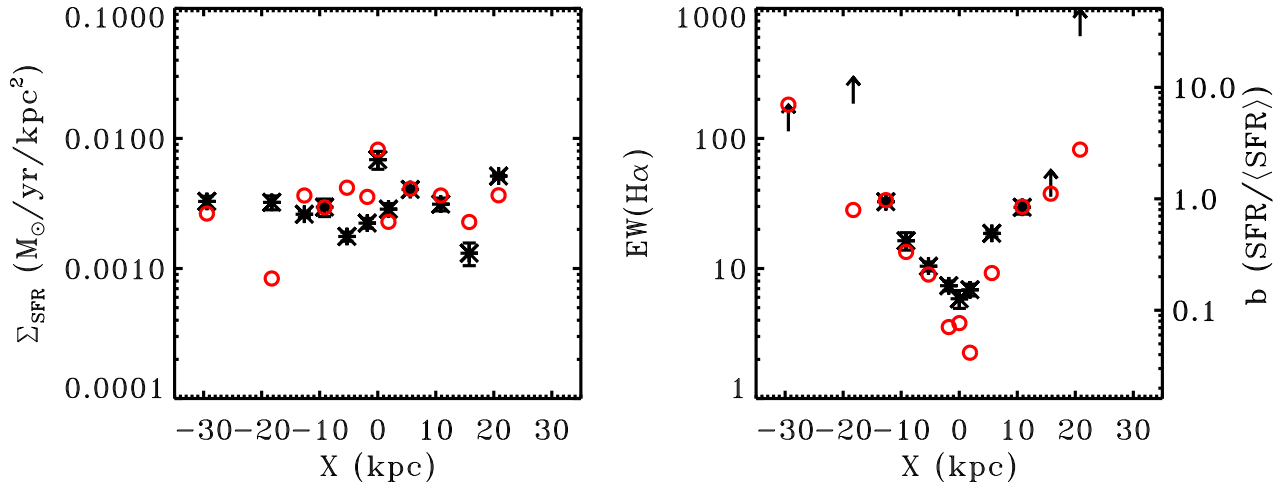


Figure 6. Left: Star formation rate surface density, in $M_{\odot} \text{ yr}^{-1} \text{ kpc}^{-2}$, as a function of radius for each spatial position across GASS35981. Black points indicate SFR surface density measured directly from dust-corrected $\text{H}\alpha$ luminosity, while red circles are estimated from fits to the photometry as described in the text. Current star formation appears to be evenly spread across the galaxy, with a scatter of only 0.2 dex. Right: $\text{EW}(\text{H}\alpha)$ as a function of position (black points and lower limits), which can be expressed as the ratio of current to past-averaged star formation, b , as described in the text. Red circles indicate b values estimated directly from the photometric fits.

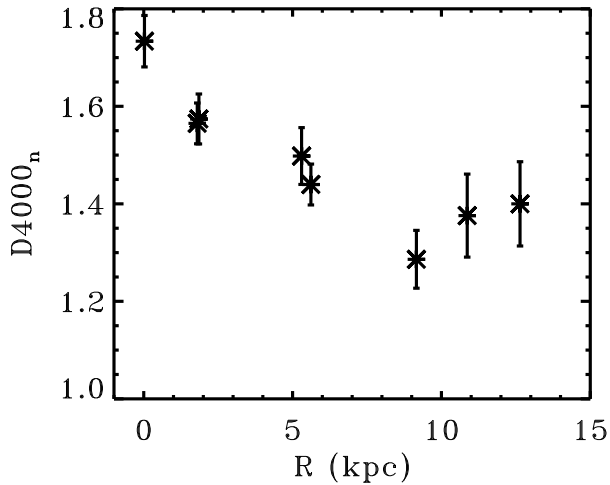


Figure 7. $D4000_n$ vs radius, with the index estimated from the best-fitting continuum model of the observed spectrum. In a simple single stellar population model from Bruzual & Charlot (2003), $D4000_n = 1.3$ indicates a stellar population age of 500 Myr, while $D4000_n = 1.7$ occurs at an age of ~ 3 Gyr.

very well. The star formation rate surface density profile of GASS35981 is quite different to those of “normal” spiral galaxies of the same stellar mass. Figure 2 of Bigiel et al. (2008) shows that in spirals where H_2 dominates in the central regions, Σ_{SFR} decreases from 0.01–0.1 $M_{\odot} \text{ yr}^{-1} \text{ kpc}^{-2}$ near the galaxy centers to less than 0.001 $M_{\odot} \text{ yr}^{-1} \text{ kpc}^{-2}$ near the edges of the optical disk. The SFR surface density profile of GASS35981 is much more similar to those of HI-dominated dwarf irregular galaxies (Figure 3 of Bigiel et al.), but these galaxies have considerably smaller stellar masses.

In the right panel of Figure 6, we plot $\text{EW}(\text{H}\alpha)$ as a function of position along the slit. Since the equivalent width is the ratio of emission line flux to the underlying continuum, it is an excellent proxy for ratio of current star formation to past-averaged star formation (i.e., pre-existing stellar mass), conventionally referred to as the b -parameter. The exact relation between the two de-

pends on the past star formation history of the galaxy. An empirical relation between the two quantities can be derived for galaxies in the SDSS using the star formation rates, stellar masses and $\text{H}\alpha$ equivalent widths published in the SDSS MPA/JHU value added catalogs¹⁴. The b -parameter is estimated from the SFRs and stellar masses using the formulation described in Brinchmann et al. (2004). We use this relation to transform between $\text{EQW}(\text{H}\alpha)$, which is plotted on the left axis of Figure 6, to b , which is plotted on the right axis of the same figure.

Figure 6 shows that the timescale for building up the current stellar mass surface density at the current star formation rate decreases strongly as a function of radius. At radii $R > 10$ kpc we find that $b > 1$, indicating that the SFR is currently higher than it has been over most of the galaxy’s history (Rocha-Pinto et al. 2000). b reaches values in excess of 10 in the very outer regions of the galaxy, indicating that all the stars in the outer disk could have been formed over a timescale as small as a few hundred Myrs.

At large radii, the $\text{H}\alpha$ emission line is very strong, but there is no detection of the underlying continuum, yielding only a lower limit on the EW. We also estimated b directly from our photometric fits, and these values are over-plotted as red circles in Figure 6. Overall, the results agree well, though there are two points where the estimated b is significantly lower than the limits implied by the spectroscopy. Reasons for the discrepancy could include small errors in sky subtraction on the spectrum leading us to underestimate the $3\text{-}\sigma$ limit on the continuum flux, which would subsequently cause an overestimate of b . Alternatively, since the discrepant points are in regions where b appears to have a strong spatial gradient, it may be that seeing and/or resolution effects are limiting how well we can match spatial extraction regions between spectrum and photometry, and the discrepancy simply reflects that spatial variation. In either case, both the spectrum and photometry agree that $b \geq 1$ all across the outer disk.

¹⁴ <http://www.mpa-garching.mpg.de/SDSS/>

Another possible worry is that b parameters and star formation rates measured through small apertures are not representative of the galaxy as a whole; however, we obtain nearly identical trends with radius when we estimate b and Σ_{SFR} from photometry that has been azimuthally-averaged in elliptical annuli across the whole galaxy.

To test whether the age of the stellar population in the outer disk is consistent with the short formation timescale deduced from the $\text{H}\alpha$ equivalent widths, we examine the radial trends in stellar population age as measured by the $D4000_n$ index (Figure 7). Although $D4000_n$ is known to vary with metallicity as well as age (Kauffmann et al. 2003), the metallicity of GASS35981 appears to be fairly uniform within the restricted range of radii over which we measure it (with only one point in Figure 7 at significantly sub-solar metallicity; see § 4.2), and so for this radial regime $D4000_n$ is the highest-S/N proxy for stellar population age that we can measure.

We see in Figure 7 that $D4000_n$ appears to decrease from ~ 1.7 in the center of the galaxy to $1.3\text{--}1.4$ beyond ~ 10 kpc. For a simple single stellar population (SSP) model from Bruzual & Charlot (2003), $D4000_n = 1.3$ indicates a stellar population age of 500 Myr, while $D4000_n = 1.7$ occurs at an age of ~ 3 Gyr. These characteristic timescales grow larger for more realistic extended star formation histories; this will be discussed further in § 5. The S/N of our spectrum is not high enough to measure $D4000_n$ at very large radii, but the fact that such young ages are implied for $R = 10$ kpc is suggestive that the outer disk may be even younger.

4.1.1. Analysis of the CO Measurements

Given the order of magnitude difference between the measured HI mass and the measured molecular gas mass, it is important to determine whether the latter is consistent with the derived star formation rate. Bigiel et al. (2008) show that SFR surface density is directly proportional to H_2 mass surface density according to the relation: $\Sigma_{\text{SFR}} = 10^{-3.1}\Sigma_{\text{H}_2}$ (in units of $M_\odot \text{ yr}^{-1} \text{ kpc}^{-2}$ and $M_\odot \text{ pc}^{-2}$, respectively). This relation holds over a large range in Σ_{H_2} ($3\text{--}50 M_\odot \text{ yr}^{-1} \text{ pc}^{-2}$) and does not appear to vary as a function of any larger scale property of the galaxies in the sample.

When comparing SFR and H_2 mass for GASS35981, we must carefully account for possible aperture effects, because the SFR surface density is measured through a narrow slit, while the H_2 masses are estimated in three much larger apertures with FWHM of $22''$. However, we have seen that in GASS35981 the SFR surface density appears to be quite uniform across the whole galactic disk. The CO line flux measured in our central pointing corresponds to an average H_2 surface density across the beam of $\Sigma_{\text{H}_2} = 3.6 \pm 0.1 M_\odot \text{ pc}^{-2}$, under our assumed conversion factor $X_{\text{CO}} = 4.4 M_\odot/L'$. Adopting the Bigiel et al. relation between Σ_{H_2} and Σ_{SFR} yields a predicted SFR surface density $\Sigma_{\text{SFR}} = 0.0029 \pm 0.0001 M_\odot \text{ yr}^{-1} \text{ kpc}^{-2}$, which is in excellent agreement with the observed Σ_{SFR} in this galaxy.

In the two offset pointings where we do not detect any CO, our most stringent upper limit (in the Northern pointing) implies that $\Sigma_{\text{H}_2} < 2.4 M_\odot \text{ pc}^{-2}$, and hence $\Sigma_{\text{SFR}} < 0.0019$. This is 50% lower than the median Σ_{SFR}

we measure from our spectra, though from Figure 6 we see that our photometric estimates of Σ_{SFR} exhibit a dip in the region covered by the northern pointing, which could explain the low H_2 mass.

Alternatively, variation in the conversion factor X_{CO} could explain the discrepancy; since below we will present evidence that the metallicity is low in the outer regions of GASS35981 (which implies a lower amount of CO per unit of H_2), this possibility seems plausible. We note that Bigiel et al. (2008) neglected variations in X_{CO} in deriving their SFR– H_2 relation, and so the ~ 0.3 dex scatter they measure likely includes a contribution from variations in metallicity/ X_{CO} . Though the single discrepant point here is too little to draw conclusions from, in a future paper we will examine possible variations in X_{CO} across the COLD GASS sample.

4.1.2. Total Star Formation Rate

Finally, we estimate a total star formation rate for GASS35981 by extrapolating the SFR surface density measured for each spectral bin along the slit to the annulus that spans the same radial range as that portion of the slit, and that extends half-way around the galaxy, where it meets the corresponding annulus extrapolated from the other side of our slit. The aperture corrections are large, but it is instructive to compare the resulting total, dust-corrected SFR with our purely photometric estimate. We find that $\text{SFR}_{\text{H}\alpha} = 3.7 \pm 0.3 M_\odot \text{ yr}^{-1}$, which is slightly higher than the value of $3.0 \pm 0.4 M_\odot \text{ yr}^{-1}$ estimated from the integrated photometry using the method described in Schiminovich et al. (2010). We find no evidence for any additional obscured component of star formation in GASS35981, as there is no counterpart in the Faint Source Catalog of IRAS (Moshir et al. 1992), to a limit of 0.2 Jy at $60 \mu\text{m}$, which corresponds to a luminosity of $L_{60} \sim 10^{10} L_\odot$.

4.2. Metallicity Gradient

We utilize the [NII] 6584 to $\text{H}\alpha$ emission line ratio as our primary metallicity indicator. We estimate metallicity from the relation of Pettini & Pagel (2004): $12 + \log(O/H) = 9.37 + 2.03 \times N2 + 1.26 \times N2^2 + 0.32 \times N2^3$ where $N2 = \log([\text{NII}]6584/\text{H}\alpha)$. The resulting metallicities are plotted as a function of position across GASS35981 in Figure 8. In the bulge and inner disk of the galaxy ($R < 15$ kpc), GASS35981 exhibits near-solar metallicity. However, at large radii, we see a sharp drop in metallicity of ~ 0.5 dex, at a radius corresponding to the start of the blue, faint outer disk of the galaxy (Figure 3). This is also the region of the galaxy where the b parameter exceeds unity.

Sharp breaks to low metallicities are not common in the portion of the larger GASS sample with follow-up MMT spectroscopy that has been analyzed so far. We find an average gradient in $\log(O/H)$ of $-0.14 \text{ dex}/r_e$, compared to $-0.41 \text{ dex}/r_e$ for GASS35981. Less than 10% of the galaxies in our sample exhibit metallicity below $12 + \log(O/H) < 8.5$, and in most of these cases, the low metallicities are seen over the whole galaxy. Only $\sim 15\%$ of the 62 galaxies analyzed so far have metallicity gradients as strong as GASS35981, and even fewer of these exhibit a sharp drop. We note that there is one well-known local galaxy with a metallicity gradient similar to GASS35981: M101 (van Zee et al. 1998). The

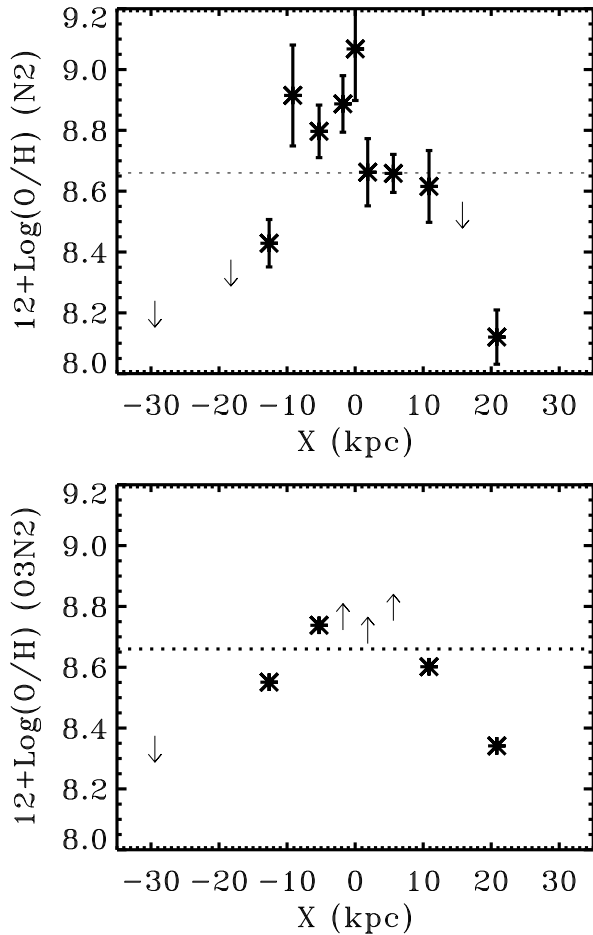


Figure 8. **Top:** Metallicity of GASS35981 as a function of position along the slit, estimated from the $[\text{NII}]/\text{H}\alpha$ emission line ratio (Pettini & Pagel 2004). Solar metallicity is marked with the dotted line. **Bottom:** Similar metallicity estimates including the ratio of $[\text{OIII}]/\text{H}\beta$, also from Pettini & Pagel, as described in the text.

importance of this similarity is unclear, however, since the two galaxies differ in other respects (e.g., the distribution of star formation; Kuntz & Snowden 2010).

As a check on our $[\text{NII}]/\text{H}\alpha$ metallicity estimates, we also compute metallicity using $\text{O3N2} = \log([\text{OIII}] 5007/\text{H}\beta/([\text{NII}] 6584/\text{H}\alpha))$ (Pettini & Pagel 2004), which is plotted in the bottom panel of Figure 8. Though intrinsically more accurate, this indicator provides somewhat poorer constraints for our galaxy, because $\text{H}\beta$ is not always detected at $> 3\sigma$ in our spectra. We note, however, that metallicities measured in this way are entirely consistent with those from $[\text{NII}]/\text{H}\alpha$, as can be seen by comparing the two panels in Figure 8. We also use $([\text{SII}] 6717 + [\text{SII}] 6731)/\text{H}\alpha$ as an additional check, as this line depends on metallicity in much the same way as $[\text{NII}]$ (Dopita et al. 2006). Although it is detected with lower S/N in our spectrum, and is more affected by sky subtraction residuals due to its redder wavelength, the $[\text{SII}]/\text{H}\alpha$ ratio exhibits a similar drop at large radii. This indicates that peculiar Nitrogen abundances are not responsible for the effect that we see.

Finally, in Figure 9 we plot metallicity as a function of $\text{EW}(\text{H}\alpha)$. There is clearly a strong correlation: regions of the galaxy with the highest ratio of current to past-averaged star formation rate are also the most metal-

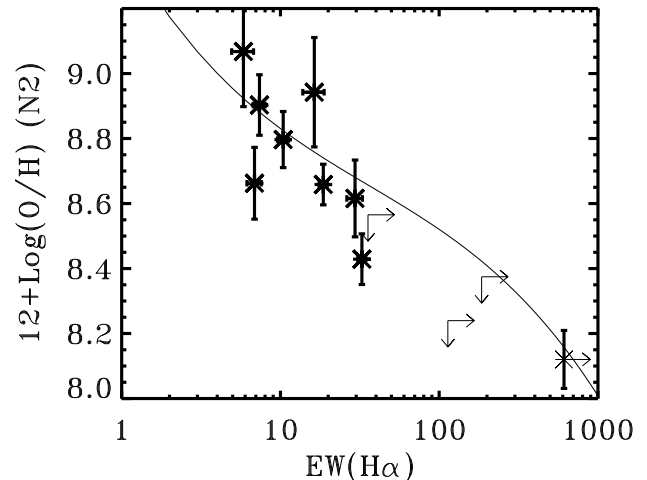


Figure 9. Metallicity from the $[\text{NII}]/\text{H}\alpha$ ratio as in Figure 8, but plotted as a function of $\text{EW}(\text{H}\alpha)$. Increasing $\text{H}\alpha$ EW is strongly correlated with decreasing metallicity in GASS35981. Solid line indicates the relation followed by normal star-forming galaxies drawn from SDSS, as described in the text.

poor. We also over-plot the best-fit relation between $\text{EW}(\text{H}\alpha)$ and $[\text{NII}]$ -based metallicity for star-forming galaxies drawn from the SDSS MPA/JHU value-added catalog. These measurements apply to the region of the galaxies sampled by the $3''$ -diameter SDSS fiber. The relation between star formation rate and metallicity measured within GASS35981 follows that exhibited by the general population of star-forming galaxies in SDSS. We note, however, that the galaxies with high $\text{EW}(\text{H}\alpha)$ and low metallicities are generally much lower mass systems.

5. DISCUSSION

We have seen that GASS35981 is currently undergoing star formation that is evenly spread across the galaxy. In the outskirts, however, a sharp drop in metallicity and a correspondingly large increase in the $\text{EW}(\text{H}\alpha)$ suggest that the bulk of the stellar mass in this region has been formed only recently, and out of a low metallicity reservoir of gas.

In this section, we ask how long ago the gas began forming its stars, and we consider the processes that may have delivered the gas to the galaxy.

5.1. A Model Star-formation History

We construct a simple toy model of the galaxy's star formation history (SFH), in the bulge ($R < 5$ kpc), inner disk ($5 < R < 15$ kpc) and outer disk ($R > 15$ kpc) of the galaxy. Using constraints derived from the galaxy's current star formation rate and stellar mass surface density, we build a simple model that is consistent with observations in all three locations.

Our observations show that the current star-formation is uniformly distributed across the galaxy, so we postulate that the overall SFH can be modeled by a period of constant star formation of some length that is the same everywhere, superimposed on an older stellar population that dominates at the center and is virtually absent at large radii.

Our model incorporates the following constraints:

- At $R > 15$ kpc, the metallicity is low and the b parameter is extremely high. Let us assume

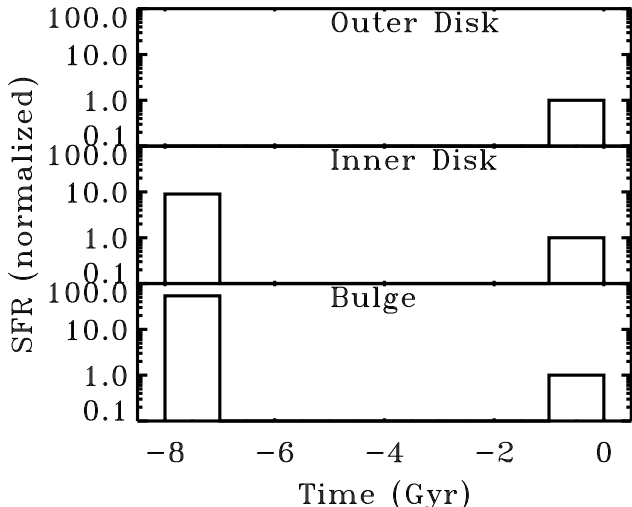


Figure 10. Schematic of a model star formation history that replicates key features of GASS35981’s stellar population in each of three radial regimes. We model the current star formation as a single episode of length 1 Gyr proceeding at the same rate everywhere across the galaxy (normalized to $SFR = 1$ in this diagram). The underlying old stellar population is modeled as another 1 Gyr-long burst occurring at $z = 1$, with amplitude constrained by the observed present-day stellar mass surface density in each radial regime.

that this indicates *all* of the existing stellar mass has been built during the current star-formation episode. For the three outer spectral bins with the lowest metallicities, the timescales for forming the entire stellar population at the currently observed star formation rate range from 0.7–2.0 Gyr. We thus adopt 1 Gyr as our reference value.

- We then subtract the stellar mass formed in the current episode from the observed stellar mass in the bulge and the inner disk, and assign the resulting mass to the old stellar population. In the inner disk, the mass surface density in the old stellar component is ~ 10 times that in the outer disk, while in the bulge region, this factor is closer to 60. For simplicity, we will concentrate all of the star formation needed to build this much mass into a single episode of 1 Gyr length ending at $z = 1$ (7 Gyr in the past).

A simple schematic of this model SFH is shown in Figure 10. We then use Bruzual & Charlot (2003) models to predict $D4000_n$ in the inner disk and bulge, obtaining values of 1.3 and 1.5, respectively. These values are in good agreement with the measured values of 1.4 and 1.6 in the corresponding radial bins. Thus, through only a simple partition of mass into old and young components, we can reasonably reproduce one of the key spectral features of GASS35981. We note that varying the formation time of the old component or doubling its timescale to 2 Gyr changes the results very little. Likewise, adjusting the length of the more recent star-forming episode within the range 0.7–2 Gyr does not significantly affect our results.

Finally, we can estimate the total fraction of the stellar mass added to the galaxy in the most recent star forma-

tion episode and find that it is around 20%. Note, however, that at its current star formation rate, GASS35981 will not exhaust its HI reservoir for another 5–7 Gyr.

5.2. Was the Gas Captured from Another Galaxy?

We have concluded that a new episode of star formation began approximately 1 Gyr ago in GASS35981. It is tempting to speculate that renewed star formation in this galaxy is connected to the acquisition of its large HI reservoir.

So how did GASS35981 acquire its gas? One possibility is that the gas was accreted as the result of an interaction with another gas-rich system. GASS35981 does have two luminous neighbors at projected distances of 300 kpc and 400 kpc with redshift differences of $< 400 \text{ km s}^{-1}$ —i.e., GASS35981 does appear to be a member of a loose group. We do not, however, see any signs of an interaction or merger in either the rotation curve or optical morphology of GASS35981.

Furthermore, a scenario in which GASS35981 is left with $2 \times 10^{10} M_{\odot}$ of HI after an encounter with either of its neighbors seems fairly implausible. Simulations predict that no more than 20% of the gas mass of any donor galaxy should be stripped in an encounter (Bournaud, private communication), so we would require a donor galaxy with $> 10^{11} M_{\odot}$ of HI! Such an encounter *could*, however, be responsible for jostling an already-present HI reservoir out of equilibrium, causing it to form stars.

If the gas was not acquired from another passing galaxy, one might speculate that GASS35981 accreted its HI reservoir directly from the surrounding intergalactic medium at some point in the past. Since blind HI surveys such as ALFALFA (Giovanelli et al. 2005) and HIPASS (Barnes et al. 2001) do not find dark HI clouds of $10^{10} M_{\odot}$, the gas must have entered GASS35981 from an ionized phase if it entered all at once or over a short timescale. Since its two identified neighbors suggest that GASS35981 resides in a group, the presence of intra-group gas could be fueling an unusually high accretion rate onto GASS35981. Indeed, accretion from the intra-group medium has been speculated to be responsible for a number of other peculiar star-forming systems (e.g., Beaulieu et al. 2010).

Alternatively, the gas reservoir could have been built slowly through multiple accretions of smaller gas clouds or streams, which could be either neutral or ionized. Under this scenario, star formation would need to be suppressed somehow during the buildup of the reservoir. The galaxy formation models of Birnboim et al. (2007) exhibit quiescent, reservoir building periods similar to what would be needed here, but in general they apply to somewhat higher mass galaxies than GASS35981, and also may not be valid at $z \sim 0$. Multiple minor mergers with gas-rich dwarfs could also supply the gas, but it becomes even harder in this case to imagine how the HI could build up over time rather than form stars with each new accretion event.

6. CONCLUSIONS

We have reported on the remarkable galaxy GASS35981, a disk galaxy with stellar mass $M_{\star} = 2 \times 10^{10} M_{\odot}$ which contains an additional $2.1 \times 10^{10} M_{\odot}$ of HI gas. Millimeter observations

indicate a molecular gas mass only a tenth this high. Through follow-up long-slit spectroscopy, plus SED fitting using our UV through optical photometry we have shown that:

- Star formation is evenly spread across the galaxy, at a surface density of $\Sigma_{\text{SFR}} = 0.003 \text{ M}_{\odot} \text{ yr}^{-1} \text{ kpc}^{-2}$.
- The proportion of the stellar mass contributed by the current star-formation episode rises towards the outer regions of the galaxy, reaching a peak at $R = 30 \text{ kpc}$, where the entire disk must have formed in the past Gyr.
- Interstellar metallicities exhibit a sharp drop at $R > 15 \text{ kpc}$, coincident with a sharp rise in $\text{EW}(\text{H}\alpha)$. This is consistent with recent infall of lower-metallicity gas (Tinsley & Larson 1978).
- The $\text{H}\alpha$ rotation curve is regular and symmetric, and reveals no signs of a recent interaction or merger that could have deposited the gas and/or triggered the recent star formation episode.

The main conclusion from our observations is that GASS35981 appears to be in the early stages of formation of its outer stellar disk.

We are not able to provide conclusive answers to questions pertaining to the origin and fate of the gas in this galaxy with this data set alone. Scenarios in which the gas was acquired in a recent merging event are disfavoured because of the extremely regular kinematics of the disk. The HI mass of GASS35981 is too large to be easily explained by gas transfer from a passing galaxy. We therefore speculate that GASS35981 acquired its gas directly from the intergalactic medium. Although our observations show that the stars in the outer disk formed within the last Gyr, this does not mean that the gas was also acquired less than 1 Gyr ago. It is also unclear whether GASS35981 will continue forming stars in its current low-efficiency state, or whether the gas will flow inwards towards the bulge, and GASS35981 will eventually develop into a more normal massive spiral galaxy with a star formation surface density that decreases as a function of radius.

Questions concerning the eventual fate of the gas can be addressed using the larger samples that will be provided by the full GASS and COLD GASS surveys in the future. By studying trends in SFR surface density, mean stellar age, metallicity, and stellar mass profiles as a function of atomic and molecular gas content for complete samples of galaxies, we hope to map out evolutionary sequences in disk galaxy formation.

Answers to questions concerning the origin of the gas will likely require a different approach. Our comparison of the HI linewidth of GASS35981 with its CO line width and $\text{H}\alpha$ rotation curve yield tantalizing hints that the atomic gas may not be in equilibrium with the rest of the galaxy. In addition, the HI spectrum in Figure 1 is clearly asymmetric about the line center. High resolution HI mapping of GASS35981 will be needed to understand the dynamical state of the gas in more detail. Even so, such observations are unlikely to prove that the HI originated from a more diffuse (and unseen) reservoir

of IGM gas. This can only be done if we are able to find tracers of this gas, for example absorption lines in the spectra of background quasars that arise when the quasar light passes through the circumgalactic medium of the galaxy (Cen & Ostriker 1999). These tracers must then be linked with galaxies like GASS35981.

The authors thank J. Brinchmann and C. Tremonti for making available their code for analysis of spectra. Based on observations carried out with the IRAM 30m telescope. IRAM is supported by INSU/CNRS (France), MPG (Germany) and IGN (Spain). The Arecibo Observatory is part of the National Astronomy and Ionosphere Center, which is operated by Cornell University under a cooperative agreement with the National Science Foundation.

Observations reported here were obtained in part at the MMT Observatory, a facility operated jointly by the Smithsonian Institution and the University of Arizona. MMT telescope time was granted by NOAO, through the Telescope System Instrumentation Program (TSIP). TSIP is funded by NSF.

Funding for the SDSS has been provided by the Alfred P. Sloan Foundation, the Participating Institutions, the National Science Foundation, the U.S. Department of Energy, the National Aeronautics and Space Administration, the Japanese Monbukagakusho, the Max Planck Society, and the Higher Education Funding Council for England.

REFERENCES

- Barnes, D. G., et al. 2001, *MNRAS*, 322, 486
 Beaulieu, S. F., Freeman, K. C., Hidalgo, S. L., Norman, C. A. & Quinn, P. J. 2010, *AJ*, 139, 984
 Bigiel, F., Leroy, A., Walter, F., Brinks, E., de Blok, W. J. G., Madore, B., & Thornley, M. D. 2008, *AJ*, 136, 2846
 Binney, J., Nipoti, C., & Fraternali, F. 2009, *MNRAS*, 397, 1804
 Birnboim, Y., Dekel, A. & Neistein, E. 2007, *MNRAS*, 380, 339
 Böhm, A., et al. 2004, *A&A*, 420, 97
 Brinchmann, J., Charlot, S., White, S. D. M., Tremonti, C., Kauffmann, G., Heckman, T., & Brinkmann, J. 2004, *MNRAS*, 351, 1151
 Bruzual, G., & Charlot, S. 2003, *MNRAS*, 344, 1000
 Calzetti, D. 2001, *PASP*, 113, 1449
 Catinella, B., Haynes, M. P., & Giovanelli, R. 2007, *AJ*, 134, 334
 Catinella, B., et al. 2010, *MNRAS*, 403, 683
 Cen, R., & Ostriker, J. P. 1999, *ApJ*, 514, 1
 Dekel, A., et al. 2009, *Nature*, 457, 451
 Dopita, M. A., et al. 2006, *ApJS*, 167, 177
 Filippenko, A., & Greenstein, J. L. 1984, *PASP*, 96, 530
 Garcia-Appadoo, D. A., West, A. A., Dalcanton, J. J., Cortese, L. & Disney, M. J. 2009, *MNRAS*, 394, 340
 Genel, S., et al. 2008, *ApJ*, 688, 789
 Giovanelli, R., et al. 2007, *AJ*, 133, 2569
 Giovanelli, R., et al. 2005, *AJ*, 130, 2598
 Kauffmann, G., et al. 2003, *MNRAS*, 341, 33
 Kauffmann, T., Mayer, L., Wadsley, J., Stadel, J., & Moore, B. 2006, *MNRAS*, 370, 1612
 Kroupa, P. 2001, *MNRAS*, 332, 231
 Kuntz, K. D. & Snowden, S. L. 2010, *ApJS*, 188, 46
 Maller, A. H., & Bullock, J. S. 2004, *MNRAS*, 355, 694
 Meurer, G. R., et al. 2009, *ApJ*, 695, 765
 Moran, S. M., Miller, N., Treu, T., Ellis, R. S., & Smith, G. P. 2007, *ApJ*, 659, 1138
 Moshir, M., Kopman, G., & Conrow, T. A. O. 1992, Pasadena: Infrared Processing and Analysis Center, California Institute of Technology, 1992, edited by Moshir, M.; Kopman, G.; Conrow, T. A. O.

- Osterbrock, D. E. 1989, *Astrophysics of Gaseous Nebulae and Active Galactic Nuclei* (Mill Valley: University Science Books)
- Oppenheimer, B. D., Davé, R., Kereš, D., Fardal, M., Katz, N., Kollmeier, J. A., & Weinberg, D. H. 2009, arXiv:0912.0519
- Peek, J. E. G., Putman, M. E., & Sommer-Larsen, J. 2008, *ApJ*, 674, 227
- Pettini, M., & Pagel, B. E. J. 2004, *MNRAS*, 348, L59
- Rocha-Pinto, H. J., Scalo, J., Maciel, W. J., & Flynn, C. 2000, *ApJ*, 531, L115
- Salim, S., et al. 2007, *ApJS*, 173, 267
- Sancisi, R., Fraternali, F., Oosterloo, T., & van der Hulst, T. 2008, *A&A Rev.*, 15, 189
- Schiminovich, D.S., 2010, *MNRAS*, submitted
- Springob, C. M. et al. 2005, *ApJS*, 160, 149
- Tinsley, B. M., & Larson, R. B. 1978, *ApJ*, 221, 554
- van Zee, L., Salzer, J. J., Haynes, M. P., O'Donoghue, A. A. & Balonek, T. J. 1998, *AJ*, 116, 2805